Sooting tendencies of ethylene diffusion flame doped by C 3 -C 5 alcohols

R. Jalain, J. Bonnety, G. Legros, A. Matynia

Version of Record: https://www.sciencedirect.com/science/article/pii/S154074892200373X
Manuscript_213b696ed5e5c605754d04968a98dfec

Sooting tendencies of ethylene diffusion flame doped by C_3-C_5 alcohols

R. Jalain[a,*], J. Bonnety[a], G. Legros[a], A. Matynia[a]

[a] *CNRS, Sorbonne Université, UMR 7190, Institut Jean Le Rond d'Alembert, Paris F-75005, France*

Abstract

The sooting propensity of steady laminar coflow ethylene/air flames is modified doping the fuel stream with vapors of alcohol and evaluated as a function of both the position of the alcohol function and the ramification level (linear/branched) of the molecule. To identify general trends, a range of 3 alcohol sizes (C_3, C_4, and C_5) are compared: the 2 propanol isomers (primary and secondary), the 4 butanol isomers (2 primaries with 1 branched, 1 secondary, 1 tertiary), and 7 pentanol isomers (3 primaries with 2 branched, 3 secondary with 1 branched and 1 tertiary). Every alcohol has been injected as a doping vapor in the central tube of a Santoro's burner. To evaluate the sooting tendencies, a Line-of-Sight Attenuation (LOSA) setup allows the extinction of a collimated laser beam operating at 645 nm to be measured yielding the field of local soot volume fraction f_v. Two indicators are used and constrasted, i.e. one using integrated data (raw data from the camera capturing the laser extinction) and one using the local field (deconvoluted data). From these results, several conclusions can be drawn. The two indicators being in good agreement, it seems unnecessary to obtain local data to compare sooting tendencies at different conditions (for a given experimental setup). The noise from the deconvolution procedure can be drastically reduced by an average filter. These results reveal a good correlation between alkene produced in rich premixed C_2H_4 flame. The sooting tendencies are consistent with the literature: linear molecule $<$ branched molecule and primary alcohol $<$ secondary alcohol $<$ tertiary alcohol. Moreover, the number of carbon N_C, here varied from 3 to 5, leads to a modification of the sooting tendency that is significantly narrower than that associated with the structure of the alcohol at a given N_C.

Keywords: non-premixed flame ; alcohol addition; alcohol isomers; soot

1. Introduction

Alcohols, such as ethanol or butanol, are promising biofuels because they can be produced by biological processes [1–4] such as ABE (acetone-butanol-ethanol) fermentation. They are also known for their ability to reduce the emissions of particulate matter [5] when mixed with conventional fuels. One of the reasons explaining this trend is the oxidizing ability of the compound, allowing for the destruction of Polycyclic Aromatic Hydrocarbons (PAHs). McEnally and Pfefferle [6] also suggested that this reduction could mainly be due to the lower number of carbons N_C of the alcohol compared to the conventional fuel. These authors evidenced that, at a given N_C, some alcohols, more specifically the secondary and tertiary ones, exhibit Yield Sooting Indices (YSIs) that are equivalent or even higher than that of the corresponding alkane.

One reason might be the preferential triggering four-center reactions, such as the elimination of water of 2-propanol:

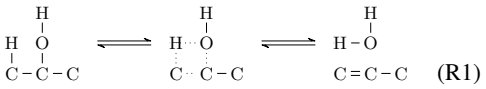
(R1)

For purposes of reducing soot formation, this reaction is very unfavorable: it sequesters the oxygen atom in an inert species and actually promotes soot formation since it converts the carbon chain into the largest possible alkene product (i.e. keeping N_C constant). The prevalence of this type of reaction has been shown for secondary and tertiary butanol isomers in diffusion flames [7] and more recently for pentanol isomers as well [8] in rich premixed flames.

Numerous studies have been dedicated to studying sooting propensities of gaseous and liquid fuel (in the standard condition of temperature and pressure) usually by doping diffusion methane flame [6, 9–11]. The variation of the sooting propensity of those flames is governed almost exclusively by the dopant chemistry [12, 13]. This configuration allows to affect sooting propensities almost exclusively to the dopant. However, as methane flames produce very few soot, this requires the use of very sensitive optical diagnostics for the evaluation of fuels with low sooting tendencies. One of the most used indicators to establish hierarchy is the Yield Sooting Index (YSI) first developed by McEnally and Pfefferle [9] which compared the $f_{v,max}$ on the symmetrical axis of the flame ($r = 0$) thanks to a scale bounded by a lower limit (lowest sooting propensities with usually $YSI = 0$ or $YSI = 30$) and a high limit (highest sooting propensities with usually $YSI = 100$). Kashif et al. [10, 11] adapted the original definition to study flame where $f_{v,max}$ is located outside the symmetrical axis (in wings of an ethylene diffusion flame for instance). They also defined a second term referred to as soot load F_v which allows reducing the eventual deconvolution noise by integrating radially the whole f_v distribution.

On the other hand, ethylene diffusion flame has been extensively studied [14–19]. Consequently soot properties of this type of flame are well-known, making it an excellent reference. It appears then interesting to take advantage of this knowledge to study the sooting tendencies of various dopants, into an ethylene flame, unveiling eventual interactions between the two fuels and making relevant Line-of-Sight Attenuation (LOSA) measurements to a various range of fuels since absorption rates, as well as signal-to-noise ratio, are higher.

To confirm the role of the oxygen atom from alcohols on sooting propensities, C_2H_4 flames, i.e. a sooting fuel with a low N_C, is investigated. To assess the importance of the alkene productions derived from alcohol on sooting propensities, the different types of alcohol are investigated, i.e. all the propanol, butanol, and 7 out of the 8 pentanol isomers, including consequently primary, secondary, and tertiary alcohols as well as linear and branched ones.

To this end, sooting propensities of ethylene axisymmetric non-premixed flames doped by 3.5% (molar, referred to as X_{vap}) of the different alcohol vapors are investigated by a Line-of-Sight Attenuation (LOSA) setup. By this technique, absorption is measured at 645 nm and soot volume fraction inferred, allowing to classify sooting propensities of the dopants with two indicators: the absorption K_0 and the soot volume fraction f_{95}, that are compared to assess the robustness of the findings.

2. Investigation configuration

2.1. Flame generation

The steady laminar diffusion flame is established over Santoro's axis-symmetric coflow burner [14]. The gas supply of the burner used is an upgraded version of the one used in Ref. [8]. Ethylene is injected via a Bronkhorst EL-FLOW mass flow controller through the vertical central brass duct, which has an 11 mm effective diameter of injection d_F. A Coriolis regulator CORI-FLOW controls the flow rate of liquid alcohol, then vaporized and mixed with ethylene with a homemade evaporator.

Two parameters are kept constant, i.e. the overall molar flowrate (hence the volumetric flowrate too) and X_{vap}. The dopant molar fraction was set at 3.5% being aligned with a recent study published by our group where alkene production was measured in rich ($\phi = 1.7$) premixed flames (C_2H_4/alcohol/air) [8]. Molar flowrate is kept constant so that inflows for all flames exhibit identical exiting velocities for fuel and air. To keep the molar flowrate constant, the C_2H_4 base flame flowrate is higher than the doped-ones (0.145 and 0.139 nl/min, respectively). All flames, in the present study, are non-smoking.

In a comparative study, the choice of the quantity to be kept constant is debatable. In the present work,

keeping the burner exit velocity constant should, theoretically, limit the variation of the flame height. However, this is not the only parameter controlling the height as carbon content in the fuel stream is another. On this point, considering an equivalent molecular formula of the mixture C_2H_4/alcohol gives $C_{2.035}H_{4.14}O_{0.035}$ for propanol, $C_{2.07}H_{4.21}O_{0.035}$ for butanol, and $C_{2.105}H_{4.28}O_{0.035}$ for pentanol. Thus, the variation of carbon content remains reasonably low (and the C/H ratio is almost constant between 0.49 and 0.5). These differences do not affect the conclusions drawn in this study. Furthermore, the major trends observed between isomers are not affected by this point. The coflowing oxidizer is air, whose mass flow rate is controlled by another Bronkhorst EL-FLOW device. The air flow is then introduced into the concentric 102 mm inner diameter brass cylinder. A perforated brass plate, glass beads, and finally a 1.2 mm cell-size 50 mm high ceramic honeycomb straighten the oxidizer flow. The fuel tube extends 6 mm above the honeycomb upper surface. Different heating sources allow maintaining the fuel temperature constant during the experiment (cf. Table 1).

Parameter				**Value**	Uncertainties
Evaporator (°C)				20-61	±2
Heated lines (°C)				80-100	±5
Fuels (°C)				65	±3
X_{vap}				0,035	$\pm 4.10^{-4}$
Air (nl/min)				30	±0.11
	ref.	prop.	but.	pent.	
C_2H_4 (nl/min)	0.145	0.139	0.139	0.139	±0.007
Alcohol (g/h)		0,818	1.009	1.201	±0.02

Table 1: Experimental parameter values.

The optimization of the methodology's discrimination potential drove the settings of the conditions investigated. The fuel flow rates have been adjusted to get the highest laminar flame that is not smoking, as the flame's tip opening that is associated with the smoke release might influence the level of soot formation upstream. Consequently, the fuel flowrate setpoint has been defined to keep the most sooting case under this threshold, i.e. the t-pentanol flame. Doing so, the Coriolis absolute error is minimized and the camera sensor captures the flame on a wide area. The air flowrate has been set to roughly match the exit velocity of the fuel. The evaporator temperature is set between 20 and 61°C. Temperatures for complete evaporation are adapted for each dopant according to the recommendations defined by the application Fluidat® of Bronkhorst. To make sure the dopant vapor feeds the ethylene flow at a constant rate, i.e. there is no accumulation effect throughout the line, a photodiode measures at a rate of 500 Hz the overall intensity of the flame. The dopant addition results in a variation of the flame radiative emission which increases the mean intensity captured by the photodiode to a level remaining very steady during the acquisition of the data.

2.2. Optical diagnostic

To measure the absorption and the emission of the flame at 645 nm, a setup (see Figure 1) similar to the one in Ref. [20] is used. Figure 1 displays the main elements. A 100 mW (± 0.5 mW) Spectra-Physics Excelsior CW Laser operating at 645 nm (-5/+7 nm) was used as the continuous light source. The selection of the wavelength is driven by the required trade-off between detection sensitivity and the small contribution of scattering to the laser extinction. Bonnety et al [18] recently demonstrated that, in the present configuration, the contribution of scattering to laser extinction was negligible at a wavelength in the range of 645 nm. Thus, scattering contribution is here neglected and extinction is considered as absorption only. Consequently, for any pixel impinged, the attenuation K_{ext} of the laser light and its absorption K_{abs} are merged.

The outcoming 1 mm diameter beam passes through a neutral density filter to adjust the incoming power to the camera, then through a Newport Oriel Electronic shutter that chops the source at a frequency of 30 Hz. After the first lens of a beam expander, a rotating glass diffuser plate combined with a vibrating one provide loss of phase to avoid the coherent effects of speckle and diffraction, which in turn enhances the spatial uniformity of the beam intensity. Finally, an achromatic lens ends the beam expander providing a 100 mm diameter collimated beam.

Once the beam has passed through the flame, the optical setup allows it to be decollimated. A pinhole with an aperture diameter of $800\,\mu\text{m} \pm 5\,\mu\text{m}$ is located at the focal point to provide a telecentric configuration possessing depth invariant magnification and to filter the beam steering due to the temperature gradient that would bias the deconvolution process. The resulting virtual image formed is re-imaged by an sCMOS pco.edge 5.5. camera mounted with a conventional lens and equipped with a narrow band filter centred at 645 nm ± 2 nm and with a 20 nm bandwidth (at one half the transmissivity maximum). This setup allows to capture the attenuated laser beam together with the flame emission through the full optical access, i.e. width of 40 mm and a height of 100 mm, with a resolution of $41\,\mu\text{m}$ per pixel for the projected data.

2.3. Data acquisition

Absorption measurement K_{abs} is done by the acquisition of a set of 4 frames constituted of $2560\,(z) \times 704\,(x)$ pixels: 1 frame with laser ON and flame established (attenuated laser light intensity I), 1 frame with the laser OFF and flame established (flame emission, I_f), 1 frame with laser ON and without flame (unattenuated laser light intensity I_0), and 1 frame without laser and without flame (background intensity, I_b). The latter two are recorded before every test. Each type of frame is acquired 150 times, then averaged and each type of flame (reference or doped one) is run 3 times, then the 3 corresponding absorption

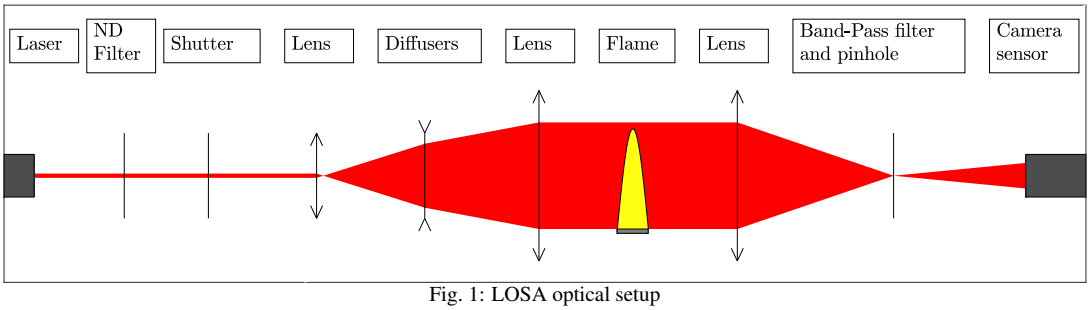

Fig. 1: LOSA optical setup

fields are averaged. The intensity standard deviation of the 450 frames is around 5%. Therefore the error range on K_{abs}, and K_0 defined in the next section, is also attributed to $\pm$ 5%.

2.4. Data processing

At a given location (x_j, z_i) , according to the Beer-Lambert law, the monochromatic transmittance of a given ray, as measured by the impinged pixel on the grid (see the LHS term in Eq. (1)), is related to the local extinction coefficient $\kappa\,(r_j, z_i)$ along the ray pathway of length L inside the flame as follows:

$$K_{abs} = -\ln\left(\frac{I - I_f}{I_0 - I_b}\right) = \int_0^L \kappa\,(r_j, z_i)\,ds \quad (1)$$

As a line-of-sight technique, LOSA needs to be combined with a subsequent deconvolution method to compute $\kappa(r_j, z_i)$ from Eq. (1). Three methods have been employed, namely the *onion-peeling* (OP), OP with Tikhonov regularization, and the Abel three points inversion. First, an onion-peeling method is performed here as it naturally takes advantage of the grid that a digital camera provides. At any z_i, the x-axis is discretized to a radial axis r (same dimension than x) and a system of linear equations Ay=b is derived from Eq. (1). y is the unknown vector of discretized $\kappa\,(r_j, z_i)$, the vector b contains the discretized RHS term of Eq. (1), and A is a matrix composed of chord lengths that can be readily calculated using simple geometrical considerations. Typically, with the optical arrangement specified above, A is a 200 $\times$ 200 matrix. A is also an upper triangular matrix, therefore y might be solved by using simple backsubstitution. However, the aforementioned set of equations can be shown to be ill-conditioned. Therefore, a subsequent Tikhonov regularization stabilized here the deconvolution process with the value of the regularization parameter Λ set to 0.5. Finally, the Abel inversion method was also applied for further comparison to assess the impact of the deconvolution method.

Once all the i lines have been processed, the Mie theory allows the soot volume fraction field $f_v\,(r_j, z_i)$ to be inferred from the $\kappa(r_j, z_i)$ one, assuming that particles are in the Rayleigh limit, by the following relation:

$$f_v\,(r_j, z_i) = \frac{\lambda\,\kappa\,(r_j, z_i)}{6\pi E(m_\lambda)} \quad (2)$$

where $E(m_\lambda)$ is a function of the complex refractive index m_λ of soot. The model of m_λ by Chang and Charalampopulos [21] is selected for the present study. Concerning the absolute value of f_v, $E(m_\lambda)$ remains one of the highest source of error: a factor up to 4 can be found for its value at 645 nm throughout the literature [22, 23]. However, since it is constant throughout the fields, it has no incidence regarding the relative values, i.e. the comparison among the flames.

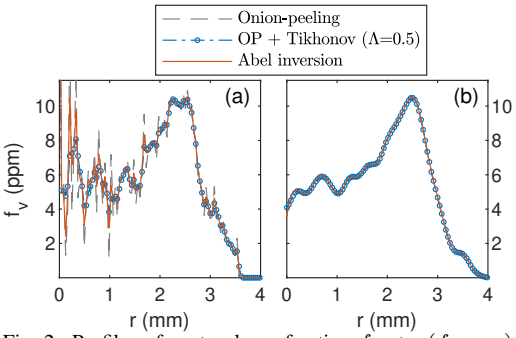

Fig. 2: Profiles of soot volume fraction f_v at $z\,(f_{v,max})$ obtained with the 3 deconvolution processings from (a) the raw field of absorption, and (b) the filtered one.

The expansion of the laser beam diameter from 1 mm to 100 mm makes the homogeneization of the backlighting difficult, especially due to the fine resolution of the camera sensor as compared to the characteristic size of the specks on the diffuser disc. Therefore, before deconvolution, an average filter is used on the raw absorption field, the 2560 $\times$ 704 grid is averaged by a 64 $\times$ 4 filter (2.63 $\times$ 0.16 mm). Doing so, the radial information is slightly spanned without smoothing significantly the strong gradient while the wider axial one is homogenized more strongly, taking advantage of the amount of pixels and the lower gradient. The impact of this filtering on the deconvolution process is displayed in Figure 2. The graphs display (a) the radial profiles of soot volume fraction at the height of the overall peak of soot volume frac-

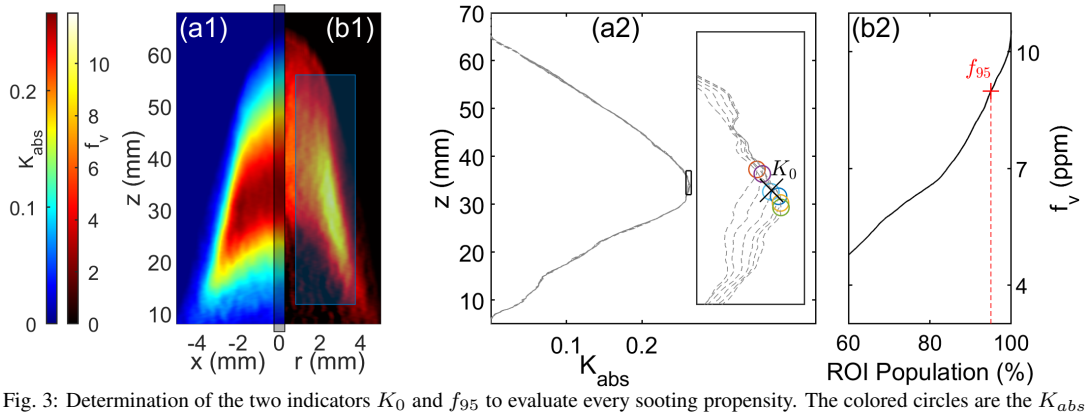

Fig. 3: Determination of the two indicators K_0 and f_{95} to evaluate every sooting propensity. The colored circles are the K_{abs} maxima of the J lines.

tion $f_{v,max}$ obtained by the 3 methods of deconvolution from the raw data and (b) the same profiles obtained from the filtered field. The high error on deconvolution process that can be seen on the Figure 2 (a) comes from laser backlight inhomogeneities combined with the high number of concentric layers (rank deficient linear system). Tikhonov regularization allows the profile to be smoothed without any significant damping of the peak. Figure 2 (b) shows that filtering the data with a proper size filter makes the field less affected by high frequency perturbations. Then, all methods are equivalent (and the regularization is unnecessary). Consequently, only results with OP deconvolution are presented in the results section.

To assess the sooting propensities of the dopants, two indicators have then been designed. The first one (see (a1) and (a2) in Figure 3) is inferred from the raw projected data and is referred to as K_0. It is the averaged value of the maximum of absorption on J columns around $x = 0$ (longest optical path L) defined as:

$$K_0 = \sum_{j=1}^{J} \frac{\max\left(K_{abs}(x_j)\right)}{J} \tag{3}$$

J is here set to 6 ($x = 0 \pm 0.1$mm).

The second indicator is extracted from the local soot volume fraction field (see Fig. 3 (b1)) and is referred to as f_{95}. Its determination first needs the cumulative population of f_v (see Fig. 3 (b1)) within the Region of Interest (ROI) encompassed between $r = 1$ mm and $r = 4$ mm, and between $z = 15$ mm and $z = 55$ mm (shaded area in Fig. 3 (b1)). f_{95} is the value of the local soot volume fraction over which stands the 95$^{\text{th}}$ centile of the sorted population. Unlike the peak soot volume fraction over the entire field, f_{95} is hardly affected by the deconvolution strategy. The procedure is also applied to the left side, i.e. $r < 0$, then f_{95} is average value of both side.

To illustrate the necessity of the procedure, Figure 4 displays the cumulative population within the ROI for every tested case. While the hierarchy between

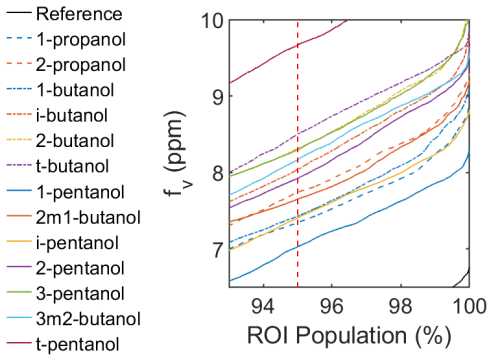

Fig. 4: Cumulative distribution of the reference flame and the doped ones.

the different alcohols is well established for cumulative populations ranging from 94 to 98%, the graph clearly shows that large and potentially non-physical variations (possibly caused by measurement artifacts) appear above 99%.

3. Results and discussion

The field of raw absorption measurements K_{abs} and local soot volume fraction f_v are presented in Figure 5. The upper row displays the fields associated with the reference flame, the 2 propanol isomers, and the 4 butanol isomers. The lower row shows the fields associated with the pentanol isomers. The isomers are sorted by type of alcohol, then by the level of ramification (i.e. primary, then secondary, and linear then branched). The reference flame exhibits the lowest sooting tendency and height. The levels of soot volume fraction measured are in the range expected for a flame with this flowrate [14, 18].

The results show that the addition of the dopant has a clear impact on the flame size. Depending on the

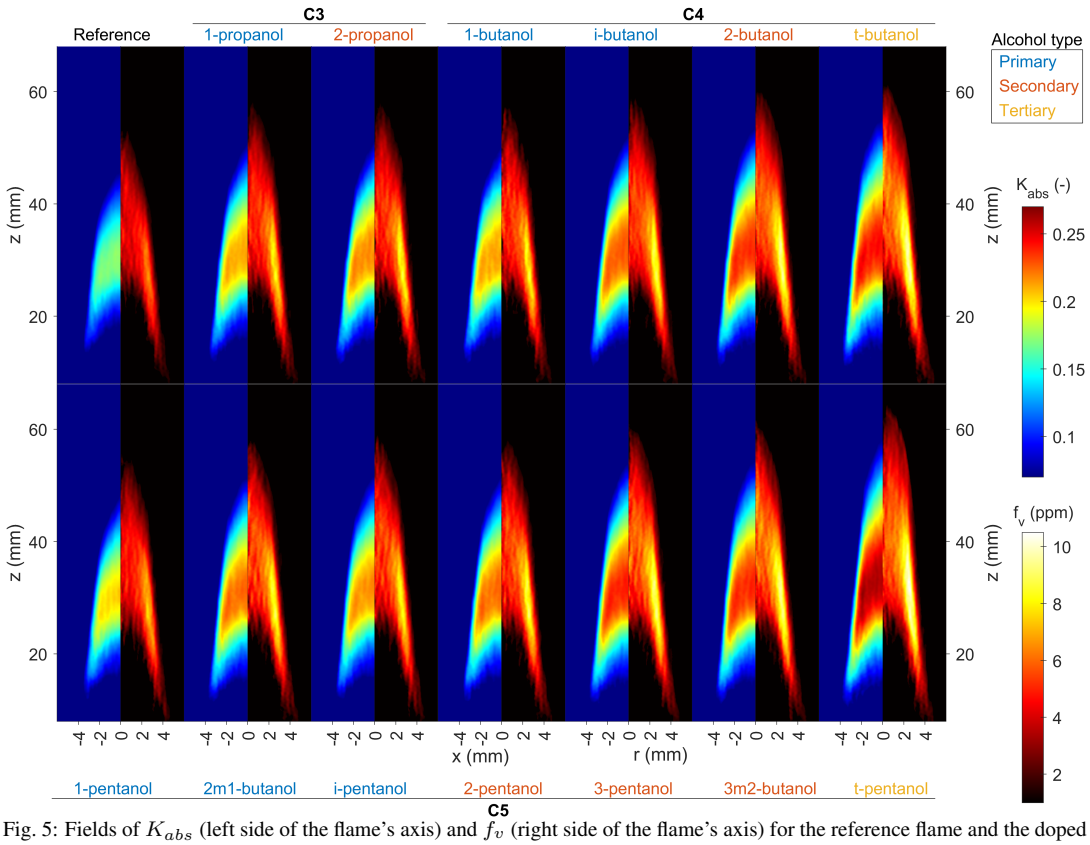

Fig. 5: Fields of K_{abs} (left side of the flame's axis) and f_v (right side of the flame's axis) for the reference flame and the doped ones.

type of alcohol added, the flame height H_f (defined by a threshold of the emission captured by the camera) can grow up to about 25% despite the relatively small amount of dopant added (3.5%), implying that a reasonable low substitution could lead to a change in chemical but also physical properties of the flame. On the contrary, flame width remains constant. Interestingly, the flame height correlates well with the indicator f_{95} defined previously and presented in detail later, as displayed in Fig. 6. While the diffusion between the oxygen from the coflow and the fuel remains identical, the quantity of soot to oxidise is higher. It could explain why, for a close-tip flame, the flame is stretched vertically with the increase of soot concentration.

Concerning the sooting tendencies, the two indicators f_{95} and K_0 allow an easier comparison among the different flames (see Fig. 7). The first important feature is the similarity between the two indicators, pointing out the dispensable interest to the deconvolution process for the classification of dopant sooting tendencies in laminar diffusion axisymmetric flame.

The addition of every dopant, including the 1-propanol (the primary alcohol with the lowest N_C among the dopants), increases the sooting tendency of ethylene. This result is in agreement with the literature since it is known that the sooting tendency may be partly correlated with the carbon number in the fuel [9]. The oxidative capacity of the alcohol function may play a role but is not sufficient to counterbalance the main trend. A discussion on potential synergistic effects is developed at the end of this section.

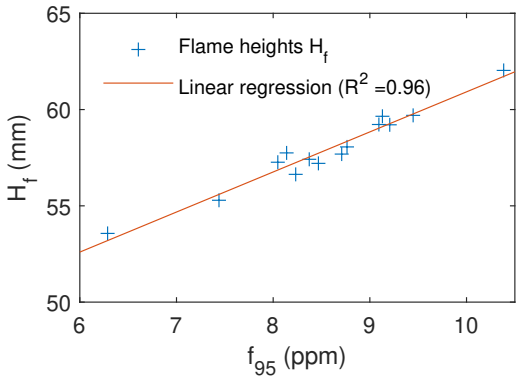

Fig. 6: Evolution of the flame height H_f with the sooting indicator f_{95}.

Surprisingly, the carbon number seems to have a minor impact on the soot production trend. For identical alcohol class, the K_0 and f_{95} indices increase slightly between propanol and butanol. The evolution between butanol and pentanol depends on the type considered: the indices decrease slightly for primary alcohols, are equivalent for secondary alcohols and increase slightly for tertiary alcohols. An inversion of the natural trend of the increasing propensity for soot production as a function of the number of carbons in the molecule is observed for primary alcohols. While this trend seems unlikely, it has to be balanced by the fact that original YSI also found a YSI lower for 1-pentanol than 2 butanol isomers, the 2- and t-butanol [24]. This find needs to be investigated in more detail and may reveal chemical interaction mechanisms during the decomposition of ethylene and alcohols. It would also be interesting to extend this work to compare the relative gain in soot production propensity when the oxygenated compound is added in a heavier fuel. Indeed, the present work suggests that the weight of the carbon number is less important than the YSI scales would suggest [24] when the main fuel is ethylene (methane being normally used for the construction of the YSI scales). Interestingly, a study concerning diesel engines found that at constant content of oxygen, the reduction could be similar for methanol, n-butanol and n-octanol [25].

Concerning isomers of the same carbon number (i.e. propanol, butanol, and pentanol), the sooting tendencies rank as follow: primary $<$ secondary $<$ tertiary and linear $<$ branched. However in the case of propanol, the difference between the two isomers remains relatively low. In the case of pentanol, 2-methyl-1-butanol (primary) and 2-pentanol (secondary) have roughly the same levels.

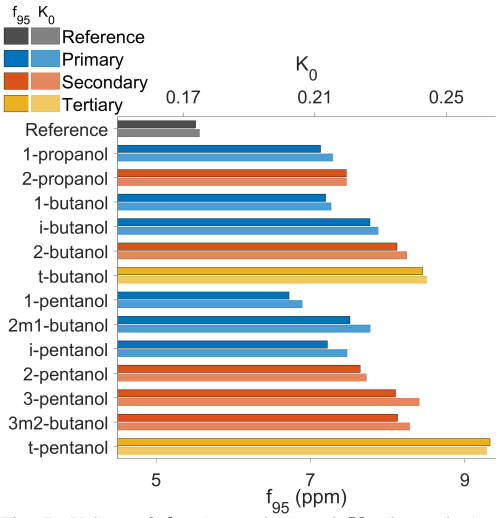

Fig. 7: Values of f_{95} (upper bar) and K_0 (lower bar) attributed to the reference flame and the doped ones.

The results on the type of alcohol are consistent with the literature [7, 8]. The results from Ref. [8] show the similar hierarchy among the alcohols concerning the production of alkenes with the number of carbon same as that of the alcohols (i.e. production of propene by propanol, butene by butanol and pentene by pentanol). Since these results are from rich premixed flames, the comparison with the current results, obtained in non-premixed flame, is not straightforward but remains relevant. Indeed, in Ref. [7], structures of non-premixed methane flames doped with the different isomers of butanol have been probed (on a Santoro burner). The concentrations of butene, species produced by the different butanol isomers, are very similar to those measured in Ref. [8]. Moreover the numerical study from this reference, carried out with several kinetic mechanisms, showed that oxygen was not involved in the formation of alkenes (C_3-C_5). Hence, linking the two types of flames seems reasonable.

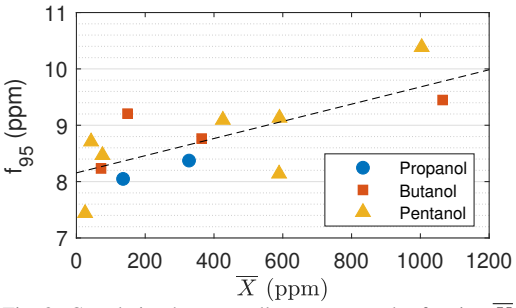

Fig. 8: Correlation between alkene mean molar fraction $\overline{X}$ obtained in rich premixed flames from Ref. [8] (respectively, propene, butene, and pentene for the flames doped in propanol, butanol, and pentanol) and the indicator f_{95}.

Figure 8 intends to assess the correlation between alkene and sooting tendency: the indicator f_{95} is plotted as a function of the average mole fraction $\overline{X}$ of the different alkenes (propene, butene and pentene). We observe that a linear regression allows to describe decently the variation of one quantity with respect to the other.

More than a simple correlation, a causal link can be supported: (i) propene, butene and pentene isomers, even if not directly identified as soot precursors, can serve as a basis for aromatic ring formation and (ii) the conversion of alcohol to alkene, in the case of dehydration (such as R1), also results in the loss of the oxygen oxidizing potential of the alcohol through the formation of non-oxidizing water (H_2O). This also suggests that the oxidative capacity of an alcohol must be strongly tempered by its structure, in particular the type of alcohol and possibly the number of branches.

The consequences of these results are important for industrial applications: doping a hydrocarbon mixture with a primary alcohol, with an equivalent number of carbons, could have a significant impact on the propensity to produce soot. In order to reduce the emission of soot particles, the effort should then focus

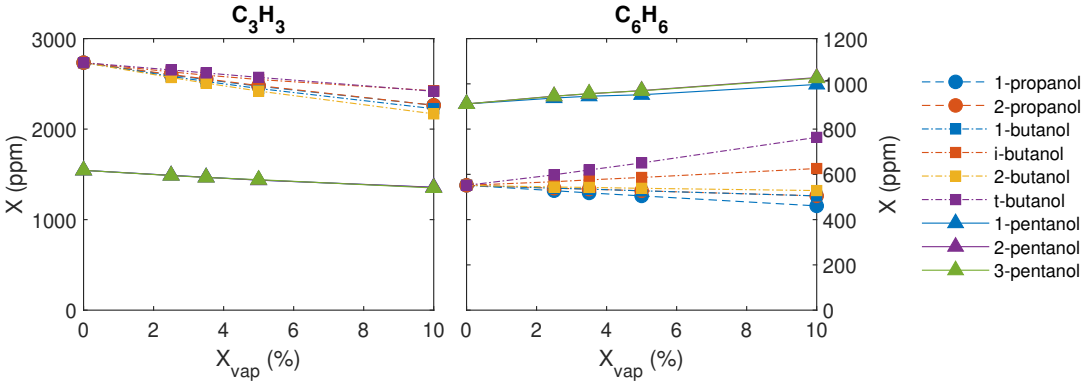

Fig. 9: Propargyl (left) and benzene (right) maximum molar fractions computed during the combustion of (C_2H_4/dopant)/air mixtures in constant pressure reactor with various molar fraction of dopant (X_{vap}). Simulations involving C_3 and C_4 alcools are performed with CRECK mechanism [26], simulation involving C_5 alcools are performed with Köhler [27] mechanism.

on the production of a primary alcohol with a higher energy content than ethanol, such as 1-pentanol.

In the view of the results, potential existence of couplings between the decomposition chemical mechanisms of ethylene and alcohols is to be questioned. A large number of works have identified synergistic phenomena between the decomposition of ethylene and dopants such as DME [28–30], ethanol [31, 32], or propane [33]. The chemical coupling mechanisms identified are associated with the production of odd-carbon number species, like for instance C_1 radicals, enhancing the production of benzene precursor species such as propargyl. Similar processes involving odd-carbon number species may also take place in PAH growth processes [33]. Numerical simulations were carried out using Cantera with Reactor model (constant pressure and enthalpy) for high equivalence ratio ($\phi = 5$) and C_2H_4/alcohol mixtures with alcohol molar fractions between 0 and 10%. Simulations are performed for temperatures of 1500 K and for times up to 1 s (composition close to thermodynamic equilibrium). The mechanism of CRECK [26] was used for propanol and butanol isomers. The mechanism of Köhler [27] was used for pentanol isomers. Maximum concentrations of C_3H_3, C_4H_6, C_2H_2, and C_6H_6 were extracted. For illustration, the results obtained with C_3H_3 and C_6H_6 are presented in Fig. 9. For all these species, the maximum concentration evolution as a function of the alcohol proportion (propanol, butanol, and pentanol isomers) is linear, suggesting an absence of coupling (or not captured by the chemical models). Future experimental measurements with progressive additions of alcohol concentration are intended to provide a better understanding of this type of phenomenon.

Interestingly, the evolution of benzene concentration follows the YSI rankings quite closely. The branched alcohols (*i*-butanol / *t*-butanol) tend to produce more C_6H_6 than the linear alcohols. The influence of branching is shown to be more pronounced in these simulations than for the experimental YSI scales and the hierarchy between *i*-butanol and 2-butanol is reversed. In view of this, the hierarchy between primary, secondary, and tertiary alcohols is also quite well reproduced.

4. Conclusion

Sooting tendencies of propanol, butanol and pentanol isomers have been evaluated as a dopant of ethylene flame in a diffusion axisymmetric configuration (Santoro burner) via LOSA at 645 nm. All dopants increased the level of soot of the pure ethylene flame. From this study, the type of molecule (type of alcohol and ramification) seems more significant than the dopant number of carbon N_C. The results point out the influence of the type of alcohol (primary/secondary/tertiary), accordingly with previous studies [7, 8]. However, the trends of soot production as a function of the carbon number are less pronounced than in the YSI scales. The present work could be pursued with an in-depth analysis in order to evaluate the possible presence of interaction between the decomposition mechanisms of ethylene and the dopant. Besides, the measurement of soot temperature could account for the variation of physical properties.

References

[1] A. F. Cann, J. C. Liao, Production of 2-methyl-1-butanol in engineered Escherichia coli, Applied Microbiology and Biotechnology 81 (1) (2008) 89–98.

[2] A. F. Cann, J. C. Liao, Pentanol isomer synthesis in engineered microorganisms, Applied Microbiology and Biotechnology 85 (4) (2010) 893–899.

[3] T. Walther, J. M. François, Microbial production of propanol, Biotechnology Advances 34 (5) (2016) 984–996.

[4] S. P. H. Azambuja, R. Goldbeck, Butanol production by Saccharomyces cerevisiae: perspectives, strategies and challenges, World Journal of Microbiology and Biotechnology 36 (3) (2020) 48.

[5] S. Kumar, J. H. Cho, J. Park, I. Moon, Advances in diesel–alcohol blends and their effects on the performance and emissions of diesel engines, Renewable and Sustainable Energy Reviews 22 (2013) 46–72.

[6] C. S. McEnally, L. D. Pfefferle, Sooting Tendencies of Oxygenated Hydrocarbons in Laboratory-Scale Flames, Environmental Science & Technology 45 (6) (2011) 2498–2503.

[7] C. S. McEnally, L. D. Pfefferle, Fuel decomposition and hydrocarbon growth processes for oxygenated hydrocarbons: butyl alcohols, Proceedings of the Combustion Institute 30 (1) (2005) 1363–1370.

[8] R. Jalain, J. Bonnety, G. Legros, A. Matynia, Doping rich ethylene premixed flames: Influence of C3 C5 alcohols on the structure of the steady one-dimensional laminar flame, Fuel 307 (2022) 121793.

[9] C. S. McEnally, L. D. Pfefferle, Improved sooting tendency measurements for aromatic hydrocarbons and their implications for naphthalene formation pathways, Combustion and Flame 148 (4) (2007) 210–222.

[10] M. Kashif, P. Guibert, J. Bonnety, G. Legros, Sooting tendencies of primary reference fuels in atmospheric laminar diffusion flames burning into vitiated air, Combustion and Flame 161 (6) (2014) 1575–1586.

[11] M. Kashif, J. Bonnety, A. Matynia, P. Da Costa, G. Legros, Sooting propensities of some gasoline surrogate fuels: Combined effects of fuel blending and air vitiation, Combustion and Flame 162 (5) (2015) 1840–1847.

[12] Y. Xuan, G. Blanquart, Numerical modeling of sooting tendencies in a laminar co-flow diffusion flame, Combustion and Flame 160 (9) (2013) 1657–1666.

[13] Q. Wang, G. Legros, J. Bonnety, C. Morin, Experimental characterization of the different nitrogen dilution effects on soot formation in ethylene diffusion flames, Proceedings of the Combustion Institute 36 (2) (2017) 3227–3235. doi:10.1016/j.proci.2016.07.063.

[14] R. J. Santoro, H. G. Semerjian, R. A. Dobbins, Soot particle measurements in diffusion flames, Combustion and Flame 51 (1983) 203–218.

[15] F. Xu, A. M. El-Leathy, C. H. Kim, G. M. Faeth, Soot surface oxidation in hydrocarbon/air diffusion flames at atmospheric pressure, Combustion and Flame 132 (1) (2003) 43–57.

[16] N. A. Slavinskaya, P. Frank, A modelling study of aromatic soot precursors formation in laminar methane and ethene flames, Combustion and Flame 156 (9) (2009) 1705–1722.

[17] Y. Wang, S. Park, S. M. Sarathy, S. H. Chung, A comparative study on the sooting tendencies of various 1-alkene fuels in counterflow diffusion flames, Combustion and Flame 192 (2018) 71–85.

[18] J. Bonnety, A. Guibaud, R. Jalain, A. Matynia, J.-L. Consalvi, F. Liu, G. Legros, Probing the local radiative quenching during the transition from a non-smoking to a smoking laminar coflow ethylene/air non-premixed flame, Combustion and Flame 203 (2019) 120–129.

[19] J. Yon, J. J. Cruz, F. Escudero, J. Morán, F. Liu, A. Fuentes, Revealing soot maturity based on multi-wavelength absorption/emission measurements in laminar axisymmetric coflow ethylene diffusion flames, Combustion and Flame 227 (2021) 147–161.

[20] M. Kashif, J. Bonnety, P. Guibert, C. Morin, G. Legros, Soot volume fraction fields in unsteady axis-symmetric flames by continuous laser extinction technique., Optics Express 20 (27) (2012) 28742–28751.

[21] H.-C. Chang, T. T. Charalampopoulos, Determination of the wavelength dependence of refractive indices of flame soot, Proc. Roy. Soc. Lond. A 430 (1880) (1990) 577–591.

[22] V. R. Stull, G. N. Plass, Emissivity of Dispersed Carbon Particles*, JOSA 50 (2) (1960) 121–129. doi:10.1364/JOSA.50.000121.

[23] T. C. Williams, C. R. Shaddix, K. A. Jensen, J. M. Suo-Anttila, Measurement of the dimensionless extinction coefficient of soot within laminar diffusion flames, International Journal of Heat and Mass Transfer 50 (7) (2007) 1616–1630. doi:10.1016/j.ijheatmasstransfer.2006.08.024.

[24] C. S. McEnally, D. D. Das, L. D. Pfefferle, Yield Sooting Index Database Volume 2: Sooting Tendencies of a Wide Range of Fuel Compounds on a Unified Scale, type: dataset (Aug. 2017).

[25] M. Pan, Y. Wang, J. Wei, H. Huang, X. Zhou, Impact of carbon chain length of alcohols on the physicochemical properties and reactivity of exhaust soot, Science of The Total Environment 799 (2021) 149434.

[26] A. Frassoldati, R. Grana, T. Faravelli, E. Ranzi, P. Oßwald, K. Kohse-Höinghaus, Detailed kinetic modeling of the combustion of the four butanol isomers in premixed low-pressure flames, Combustion and Flame 159 (7) (2012) 2295–2311.

[27] M. Köhler, T. Kathrotia, P. Oßwald, M. L. Fischer-Tammer, K. Moshammer, U. Riedel, 1-, 2- and 3-Pentanol combustion in laminar hydrogen flames – A comparative experimental and modeling study, Combustion and Flame 162 (9) (2015) 3197–3209.

[28] C. S. McEnally, L. D. Pfefferle, The effects of dimethyl ether and ethanol on benzene and soot formation in ethylene nonpremixed flames, Proceedings of the Combustion Institute 31 (1) (2007) 603–610.

[29] B. A. V. Bennett, C. S. McEnally, L. D. Pfefferle, M. D. Smooke, M. B. Colket, Computational and experimental study of the effects of adding dimethyl ether and ethanol to nonpremixed ethylene/air flames, Combustion and Flame 156 (6) (2009) 1289–1302.

[30] T. Li, T. Mitra, C. Chu, Y. Yuan, M. J. Thomson, Investigation of PAH and soot formation in a dimethyl ether (DME) laminar coflow diffusion flame, Combustion and Flame 223 (2021) 437–449.

[31] F. Yan, L. Xu, Y. Wang, S. Park, S. M. Sarathy, S. H. Chung, On the opposing effects of methanol and ethanol addition on PAH and soot formation in ethylene counterflow diffusion flames, Combustion and Flame 202 (2019) 228–242.

[32] S. S. Yang, L. Gülder, Ethanol supplement increases soot yields in nitrogen-diluted laminar ethylene diffusion flames at pressures from 3 to 5 bar, Combustion and Flame 227 (2021) 1–10.

[33] J. Y. Hwang, S. H. Chung, W. Lee, Effects of oxygen and propane addition on soot formation in counterflow ethylene flames and the role of C3 chemistry, Symposium (International) on Combustion 27 (1) (1998) 1531–1538.